DROOPY LEAF1 controls leaf architecture by orchestrating early brassinosteroid signaling

Meicheng Zhao[a,b,1], Sha Tang[b,1], Haoshan Zhang[b,1], Miaomiao He[b,c], Jihong Liu[b,d], Hui Zhi[b], Yi Sui[b], Xiaotong Liu[b], Guanqing Jia[b], Zhiying Zhao[d], Jijun Yan[e,f], Baocai Zhang[e,f], Yihua Zhou[e,f], Jinfang Chu[e,f], Xingchun Wang[c], Baohua Zhao[d], Wenqiang Tang[d], Jiayang Li[e,f], Chuanyin Wu[b,2], Xigang Liu[d,g,2], and Xianmin Diao[b,2]

[a]Key Laboratory of Agricultural Water Resources, Hebei Laboratory of Agricultural Water-Saving, Center for Agricultural Resources Research, Institute of Genetics and Developmental Biology, The Innovative Academy of Seed Design, Chinese Academy of Sciences, 050021 Shijiazhuang, China; [b]Institute of Crop Sciences, Chinese Academy of Agricultural Sciences, 100081 Beijing, China; [c]College of Life Sciences, Shanxi Agricultural University, Taigu, 030801 Shanxi, China; [d]Ministry of Education Key Laboratory of Molecular and Cellular Biology, Hebei Collaboration Innovation Center for Cell Signaling, Hebei Key Laboratory of Molecular and Cellular Biology, College of Life Sciences, Hebei Normal University, 050024 Shijiazhuang, China; [e]State Key Laboratory of Plant Genomics, and National Center for Plant Gene Research (Beijing), Institute of Genetics and Developmental Biology, The Innovative Academy of Seed Design, Chinese Academy of Sciences, 100101 Beijing, China; [f]University of Chinese Academy of Sciences, 100039 Beijing, China; and [g]State Key Laboratory of Plant Cell and Chromosome Engineering, Center for Agricultural Resources Research, Institute of Genetics and Developmental Biology, The Innovative Academy of Seed Design, Chinese Academy of Sciences, 050021 Shijiazhuang, China

Edited by Cyril Zipfel, University of Zurich, Zurich, Switzerland, and accepted by Editorial Board Member Joseph R. Ecker July 16, 2020 (received for review February 6, 2020)

Leaf architecture directly determines canopy structure, and thus, grain yield in crops. Leaf droopiness is an agronomic trait primarily affecting the cereal leaf architecture but the genetic basis and underlying molecular mechanism of this trait remain unclear. Here, we report that DROOPY LEAF1 (DPY1), an LRR receptor-like kinase, plays a crucial role in determining leaf droopiness by controlling the brassinosteroid (BR) signaling output in *Setaria*, an emerging model for Panicoideae grasses. Loss-of-function mutation in DPY1 led to malformation of vascular sclerenchyma and low lignin content in leaves, and thus, an extremely droopy leaf phenotype, consistent with its preferential expression in leaf vascular tissues. DPY1 interacts with and competes for SiBAK1 and as a result, causes a sequential reduction in SiBRI1–SiBAK1 interaction, SiBRI1 phosphorylation, and downstream BR signaling. Conversely, DPY1 accumulation and affinity of the DPY1–SiBAK1 interaction are enhanced under BR treatment, thus preventing SiBRI1 from overactivation. As such, those findings reveal a negative feedback mechanism that represses leaf droopiness by preventing an overresponse of early BR signaling to excess BRs. Notably, plants overexpressing DPY1 have more upright leaves, thicker stems, and bigger panicles, suggesting potential utilization for yield improvement. The maize ortholog of DPY1 rescues the droopy leaves in *dpy1*, suggesting its conserved function in Panicoideae. Together, our study provides insights into how BR signaling is scrutinized by *DPY1* to ensure the upward leaf architecture.

plant architecture | leaf droopiness | brassinosteroid signaling | negative feedback regulation

The leaf is the primary organ for the capture of light and organic compound synthesis in plants. For cereal crops, leaf architecture is an important agronomic trait that directly determines canopy structure, as well as grain yield (1, 2). Modern commercial varieties of those crops, including maize (*Zea mays*), rice (*Oryza sativa*), and sorghum (*Sorghum bicolor*), have been developed for an erect leaf architecture that facilitates high-density cropping for efficient light capture. Despite the success of breeding erect leaf varieties, the molecular mechanisms governing the control of leaf architecture are largely unknown.

Cereal plants have long narrow leaves. The leaf angle, arc from the leaf midrib to the stem above it, and blade strength are the primary determinants of leaf architecture. In rice, mutants of various genes involved in either brassinosteroid (BR) synthesis or BR signaling display smaller leaf angles due to an increased cell number at the abaxial side of the blade/sheath boundary (3), but the associated pleiotropic effects, including dwarfism and smaller grains, hinder their application in breeding programs (4). In maize, the *Upright Plant Architecture 2* allele, from its ancestor teosinte, has been shown to reduce leaf angle by regulating the endogenous BR content (2). The rice *DROOPING LEAF* and maize *drooping leaf1* (*drl1*) and *drl2* are YABBY genes reported so far to control leaf blade strength by influencing midrib development (1, 5). Mutants of those genes exhibit an extremely droopy phenotype, in addition to other pleiotropic defects. The angiosperm-specific *YABBY* family members of transcriptional factors are important players in leaf lamina development, such as for the establishment of leaf polarity in *Arabidopsis* (6). However, the molecular mechanisms underlying blade strength control remain to be elucidated.

Brassinosteroids are a class of steroid hormones with wide-ranging effects on almost all of the aspects of plant growth and development (4, 7). The BR signaling pathway has been extensively studied in *Arabidopsis* and its key components compose a cascade (8). BRs bind to the ectodomain of its receptor BRASSINOSTEROID-INSENSITIVE1 (BRI1) (9). Ligand perception induces heterodimerization between BRI1 and its coreceptor BRI1-ASSOCIATED

Significance

C_4 cereals in subfamily Panicoideae typically produce large and long leaf blades for efficient capture of light and photosynthesis but the leaves droop downward, particularly at the adult stage, thus, adversely affecting canopy structure and grain yield. Identification of key regulators that control leaf droopiness is crucial to improve plant architecture in these crops. We showed that DPY1, a regulator of SiBRI1–SiBAK1 interaction, prevents BR signaling from overactivation in response to high doses of BRs to ensure that the long leaf blades grow upward in *Setaria*. Overexpressing DPY1 improves plant architecture with upright leaves. This study provides cellular and molecular insights into plant architecture control for cereal breeding.

Author contributions: J. Li, C.W., Xigang Liu, and X.D. designed research; M.Z., S.T., H. Zhang, M.H., J. Liu, H. Zhi, Y.S., Xiaotong Liu, G.J., Z.Z., J.Y., B. Zhang, and X.D. performed research; M.Z., S.T., Y.Z., J.C., X.W., B. Zhao, W.T., C.W., and X.D. analyzed data; and M.Z., C.W., Xigang Liu, and X.D. wrote the paper.

The authors declare no competing interest.

This article is a PNAS Direct Submission. C.Z. is a guest editor invited by the Editorial Board.

[1]M.Z., S.T., and H. Zhang contributed equally to this work.

[2]To whom correspondence may be addressed. Email: wuchuanyin@caas.cn, xgliu@sjziam.ac.cn, or diaoxianmin@caas.cn.

This article contains supporting information online at https://www.pnas.org/lookup/suppl/doi:10.1073/pnas.2002278117/-/DCSupplemental.

KINASE1 (BAK1), forming a stable high-affinity complex through their leucine-rich repeat (LRR) domains (10–13). This allows proximity of the intracellular kinase domains that transphosphorylate each other (14–16), resulting in BRI1 activation and BRI1 kinase inhibitor (BKI1) dissociation (17). Then, BR-activated BRI1 modulates a cascade of kinases and phosphatases to transduce signaling from the cell membrane to the cytoplasm (8, 18, 19), where the key node transcription factors BRASSINAZOLE-RESISTANT1 (BZR1) and BRI1-EMS-SUPPRESSOR1 (BES1/BZR2) are dephosphorylated, and move into the nucleus to activate global BR responses (20, 21). While intense signaling activity is presumably essential for the initiation of signaling transduction, several lines of evidence show that feedback regulation at the signal perception stage is crucial for proper signal output and normal plant development. For example, a SUPPRESOR of BRI1 (SBI1)–Protein Phosphatase 2A (PP2A) complex located on the plasma membrane has been shown to negatively regulate early BR signaling by inactivating BRI1 (22, 23). BR induces SBI1 expression, which, in turn, promotes PP2A to associate with plasma membrane, where it selectively dephosphorylates/inactivates BR-activated BRI1 to maintain a proper signal output. The importance of feedback regulation in early BR signaling is less documented in cereal plants, especially with regard to leaf blade development.

Here, we used foxtail millet (*Setaria italica*), a new model species for C_4 and the Panicoideae grasses (24, 25), to study leaf architecture control. We isolated a droopy leaf mutant, namely, *droopy leaf 1* (*dpy1*). DPY1 represses early BR signaling to release BR inhibition on the proliferation of both clear cells and abaxial sclerenchyma cells in leaf veins and lignin deposition in leaf blades, thus supporting the upright leaf architecture. Our findings fine tune a mechanism that governs BRI1 activity in a tissue-specific manner and show possibility to use a BR signaling modulator for crop improvement.

Results

***dpy1* Shows Droopy Leaf Associated with Increased Sensitivity to BL Treatment.** To investigate the developmental control of leaf architecture in foxtail millet, we performed ethyl methanesulfonate mutagenesis using the variety Yugu1 (wild type [WT]). We isolated a mutant that showed the most dramatically curved-down leaves in seedlings, while the leaves of WT seedlings were upright (Fig. 1*A*). The leaf phenotype developed as the mutant plant grew and became fully droopy after heading (Fig. 1*B*), whereas the leaf-stem angle of the mutant was only slightly larger than that of the WT (*SI Appendix*, Fig. S1), indicating that the leaf blade rather than the laminar joint is mainly responsible for the droopy phenotype in the mutant. Moreover, the mutant leaves were smaller, with a significant reduction in blade width (*SI Appendix*, Fig. S1). Therefore, the mutant was named *droopy leaf1* (*dpy1*). Additionally, *dpy1* was susceptive to pathogen attack in the field (*SI Appendix*, Fig. S2). The midrib plays a pillar role in supporting the upward leaf architecture in monocot plants (1, 5). We found that the *dpy1* mutant had a thinner midrib (Fig. 1*C*). Further transverse section analysis showed that the number of large clear cells and cells in abaxial sclerenchyma decreased dramatically in *dpy1*, coupled with smaller vascular tissues and reduced lignin deposition, as shown by phloroglucinol-HCl staining (Fig. 1 *D*–*G*). Consistently, cell wall analysis of whole leaf blades indicated a reduction in most of the measured compositions, including lignin that is critical for cell wall rigidity (*SI Appendix*, Table S1). This anatomic defect in the *dpy1* midrib calls for the role of BRs in inhibiting abaxial sclerenchyma cell proliferation in rice leaf joints, which results in an enlarged stem-leaf angle (3). Then, *dpy1* seeds were germinated in the dark to determine any changes in skotomorphogenesis and found stronger stimulation of coleoptile elongation relative to the WT (Fig. 1*H*). We therefore further investigated response of *dpy1* to treatment with brassinolide (BL), the most active BR, in coleoptile elongation when grown in the dark. A stimulation effect of BL on coleoptile elongation was seen at a concentration as low as 0.01 nM and an inhibition effect at 10 nM in *dpy1* (Fig. 1*I*), whereas the corresponding effects in the WT were seen at 100-fold higher concentrations, indicating enhanced sensitivity to BL in *dpy1*. Conversely, when treated with BRZ (an inhibitor of BR synthesis), coleoptile elongation was inhibited starting at 5 nM in the WT, whereas a similar inhibition in *dpy1* started at a 100-fold higher concentration (Fig. 1*I*). These findings suggest the involvement of *DPY1* in BR signaling.

DPY1 Encodes a Plasma Membrane-Located Leucine-Rich Repeat Receptor Kinase (LRR-RK) and Functions Conservatively in the Panicoideae Subfamily. By map-based cloning and MutMap analysis, a point mutation was identified in the third intron of *Seita.5G121100*, resulting in a premature stop codon in the *dpy1* transcript (Fig. 2 *A* and *B* and *SI Appendix*, Fig. S3). Thus, *Seita.5G121100* was locked in as a candidate for *DPY1*. To verify if *Seita.5G121100* is *DPY1*, the CRISPR/Cas9 system was used to knock out *Seita.5G121100* in WT plants. Two independently edited plants (CR-1 and CR-4) were generated (*SI Appendix*, Fig. S4*A*), which phenocopied *dpy1*, showing conspicuously droopy leaves at the seedling stage and completely drooped leaves at the heading stage (Fig. 2*C* and *SI Appendix*, Fig. S4*B*). The droopy leaves of *dpy1* were rescued by transformation with a 7.0-kb *Seita.5G121100* genomic fragment fused to *GFP* (Fig. 2*C* and *SI Appendix*, Fig. S4*C*). Thus, *Seita.5G121100* is responsible for *DPY1*. Overexpression of *FLAG*-tagged *DPY1*, under control of the strong maize *Ubiquitin-1* promoter (*Ubi::DPY1-3FLAG*), resulted in more upward leaf architecture, a thicker stem, and more grains per panicle without a compromise in grain weight, compared to the WT (*SI Appendix*, Fig. S5), indicating the potential for crop improvement by manipulating *DPY1* expression. Phylogenetic analysis revealed that DPY1, an ortholog of *Arabidopsis* NSP-interacting kinase 3 (NIK3), is a member of subfamily II of LRR-RKs and evolutionarily conserved in dicot and monocot species (*SI Appendix*, Fig. S6*A*). Two *DPY1* homologs were found in maize (*GRMZM2G010693*/*GRMZM2G067675*) (*SI Appendix*, Fig. S6*A*). We cloned *GRMZM2G010693* and overexpressed it under control of the *Ubiquitin-1* promoter (*Ubi::ZmDPY1-3FLAG*) in *dpy1*. The droopy leaf was fully rescued in the transgenic plants (Fig. 2*C* and *SI Appendix*, Fig. S4*D*), suggesting the conserved function of *DPY1* between species in the Panicoideae subfamily.

Protein structure analysis predicted that DPY1 contains a signal peptide at the N terminus, followed by five tandem LRRs, a transmembrane domain, and a serine/threonine protein kinase domain (*SI Appendix*, Fig. S6*B*), suggesting that DPY1 is likely a putative transmembrane kinase protein. Confocal imaging of foxtail millet leaf protoplasts transiently expressing *35S::DPY1-GFP* showed clear plasma membrane localization of DPY1-GFP (Fig. 2*D*). qRT-PCR analysis showed that *DPY1* had the highest expression in leaf blades (Fig. 2*E*). Histochemical analysis of *DPY1::GUS* transgenic leaf blades (*DPY1* promoter fused to β-glucuronidase) revealed vasculature-preferential GUS activity (Fig. 2 *F* and *G*). This expression profile was recaptured in plants carrying DPY1-GFP fusion, driven by the *DPY1* promoter (Fig. 2*H*), supporting the role of DPY1 in vascular tissue development.

DPY1 Directly Interacts with SiBAK1, but Not SiBRI1, in a Partial Phosphorylation-Dependent Manner. To study how DPY1 functions, an immunoprecipitation (IP) assay with an anti-FLAG antibody was performed using *Ubi::DPY1-3FLAG* transgenic foxtail millet, followed by liquid chromatography-tandem mass spectrometry (MS) analysis to isolate DPY1-interacting proteins. A list of putative DPY1-interacting proteins was identified, including XP_004972726, an ortholog of the BR coreceptor BAK1 (*SI Appendix*, Table S2). Since DPY1 may be involved in BR signaling, as indicated by the changed sensitivity of *dpy1* to BL or BRZ treatment (Fig. 1*I*), we chose XP_004972726, named

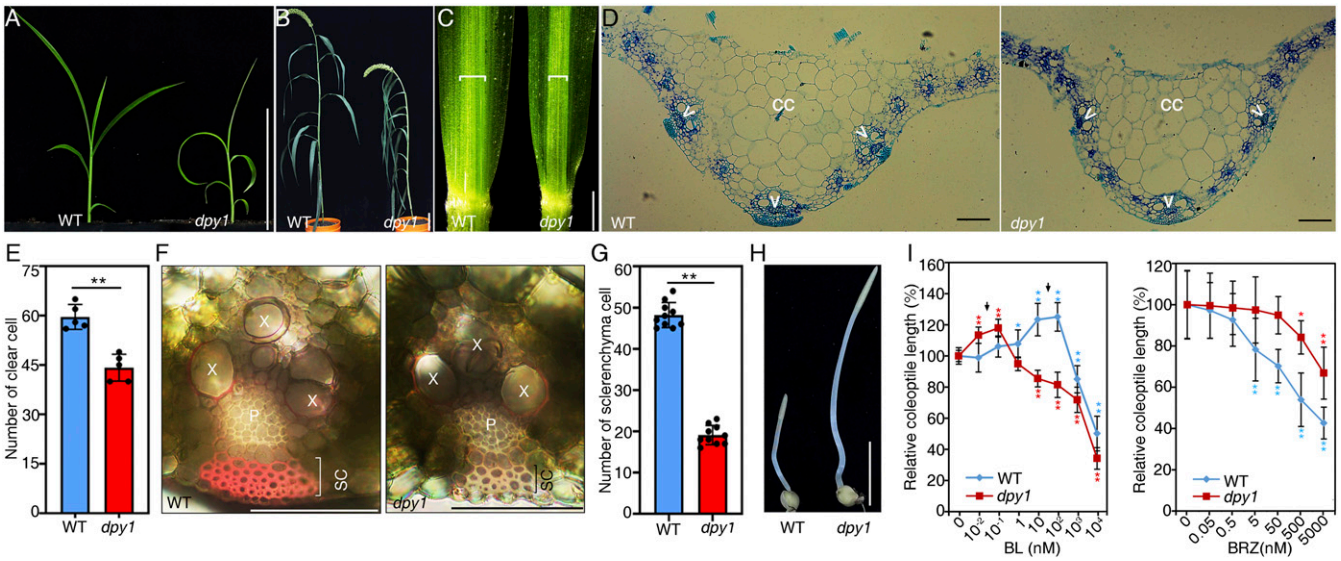

Fig. 1. Morphological and physiological characterization of *dpy1*. (*A* and *B*) Gross morphology of *dpy1* and WT plants at the seedling (*A*) and adult (*B*) stages. (Scale bar, 10 cm.) (*C*) Abaxial surface of an adult leaf, showing the narrower midrib in *dpy1*. Downward brackets denote the midrib. (Scale bar, 1 cm.) (*D*) Transverse section of the midrib at 5 cm distal to the blade-sheath joint of an adult leaf, showing few clear cells and less organized veins in *dpy1* (*Right*) than in the WT (*Left*). CC, clear cells; V, vascular bundles. (Scale bar, 100 μm.) (*E*) Quantification of clear cells in the midribs of the WT and *dpy1*. Data are presented as the mean ± SD (SD) ($n = 5$). $^{**}P < 0.01$ (Student's *t* test). (*F*) Cross-sections of the midrib of leaf blades at 5 cm distal to the blade-sheath boundary, showing fewer sclerenchyma cells (SCs) and smaller phloem (P) and xylem (X) areas in *dpy1* (*Right*) than in the WT (*Left*). Lignin staining of *dpy1* SCs with phloroglucinol-HCl (red) indicates *Lower* lignin content relative to the WT. (Scale bars, 100 μm.) (*G*) Quantification of SCs. Error bars indicate the SD ($n = 10$). $^{**}P < 0.01$ (Student's *t* test). (*H*) Enhanced elongation of the *dpy1* coleoptile in response to darkness. Plants were germinated in the dark for 5 d. (Scale bar, 1 cm.) (*I*) Increased sensitivity to brassinolide (BL) (*Left*) and reduced sensitivity to BRZ (BR synthesis inhibitor) (*Right*) treatments in *dpy1* compared with the WT, as measured by coleoptile elongation of the dark-grown seedlings. Error bars indicate the SD ($n = 10$). The average coleoptile length of the mock-treated plants (0 nM BL) was set as 100%. Arrows indicate elongation peaks of WT and *dpy1* coleoptiles as a result of BL treatment. $^{*}P < 0.05$, $^{**}P < 0.01$ (Student's *t* test).

SiBAK1, as the best candidate for further study. To confirm the DPY1–SiBAK1 interaction, coimmunoprecipitation (Co-IP) analysis was then performed using foxtail millet leaf protoplasts cotransfected with *35S::SiBAK1-HA* and *35S::DPY1-GFP* constructs and found that DPY1 coimmunoprecipitated with SiBAK1 (Fig. 3*A*). Their association was further verified by a bimolecular fluorescence complementation (BiFC) assay in *Nicotiana benthamiana* (Fig. 3*B*). We then tested whether DPY1 directly interacts with BAK1 in an in vitro pull-down assay. Given that BAK1 is known to interact with its partner proteins through their respective kinase domains (KDs) (26), the KDs of DPY1 and SiBAK1 were purified and fused with His and MBP tag, respectively. A pull-down assay showed that SiBAK1-KD interacted with DPY1-KD (Fig. 3*C*), indicating that DPY1 and SiBAK1 directly interact through their KDs. Moreover, the interaction between DPY1 and SiBAK1 was also seen in a split-ubiquitin membrane-based yeast two-hybrid system (Fig. 3*D*). The yeast growth results showed that DPY1 interacted with SiBAK1, but not SiBRI1 (Fig. 3*D*). Introduction of a mutation into the kinase domain of DPY1 compromised the interaction to a level detectable by a pull-down assay (*SI Appendix*, Fig. S7), but not by the Y2H assay (Fig. 3*D*). These findings demonstrated that DPY1 kinase activity or phosphorylated status contributes to the interaction with SiBAK1.

DPY1 Represses BR Signaling and Prevents Leaf Droopiness by Competing with SiBRI1 for SiBAK1. Since the BRI1–BAK1 association upon BR binding initiates early BR signal transduction and DPY1 physically interacts with SiBAK1 as shown above, we hypothesized that DPY1 represses BR signaling by diminishing the BRI1–BAK1 interaction. An in vitro pull-down assay was then performed to examine the competition between DPY1 and SiBRI1 for SiBAK1. The results showed that SiBAK1 and SiBRI1 interacted with each other through their KDs, consistent with previous reports in other species (13), and such interactions were weakened by the addition of DPY1-KD in a dosage-dependent manner (Fig. 4*A*). Next, we transiently expressed *35S::SiBAK1-HA* in foxtail millet leaf protoplasts of *dpy1* and WT, respectively, precipitated protein complexes containing SiBAK1-HA with the anti-HA antibody, and examined the amount of coprecipitated SiBRI1 with the anti-SiBRI1 antibody that had been validated (*SI Appendix*, Fig. S8*A*). When an equal amount of precipitated SiBAK1-HA was loaded, a remarkable increase in coprecipitated SiBRI1 was detected from *dpy1*, relative to that from WT (Fig. 4*B* and *SI Appendix*, Fig. S9*A*), demonstrating an enhanced in vivo SiBRI1–SiBAK1 interaction in *dpy1*. We expected that enhancement of the SiBRI1–SiBAK1 interaction in *dpy1* would enhance transphosphorylation and, in turn, increase phosphorylated SiBRI1. To test this, we immunoprecipitated endogenous SiBRI1 with anti-SiBRI1 antibody to detect the phosphorylation level of SiBRI1 by Western blotting with the anti-pThr antibody. The outcome showed that phosphorylation of SiBRI1 was enhanced in *dpy1* (Fig. 4*C* and *SI Appendix*, Fig. S9*B*). To further confirm elevated BR signaling in *dpy1*, the in vivo phosphorylation status of SiBZR1 (Seita.2G367800.1), a foxtail millet ortholog of BZR1 that is a key downstream component in transducing the BR signal upon dephosphorylation, was examined. We first confirmed the functionality of SiBZR1 by creating SiBZR1-overexpressing plants that displayed droopy leaves, a phenotype similar to that of *dpy1* (*SI Appendix*, Fig. S10). The dephosphorylated SiBZR1 isoform was significantly elevated in *dpy1*, to a level detected in the WT when treated with BL at 1 μM (Fig. 4*D* and *SI Appendix*, Fig. S8 *B* and *C*), indicating enhanced BR signaling in *dpy1*. Correspondingly, RNA-seq analysis revealed 5,276 differentially expressed genes (DEGs) in *dpy1* and 4,108 DEGs in the BL-treated WT, compared with the mock-treated WT control (*SI Appendix*, Fig. S11 *A* and *B*), in which 2,009 and 1,498 putative BZR1 target genes, respectively, were identified. Roughly half of these BZR1 target genes (714 of 1,498) in the BL-treated WT

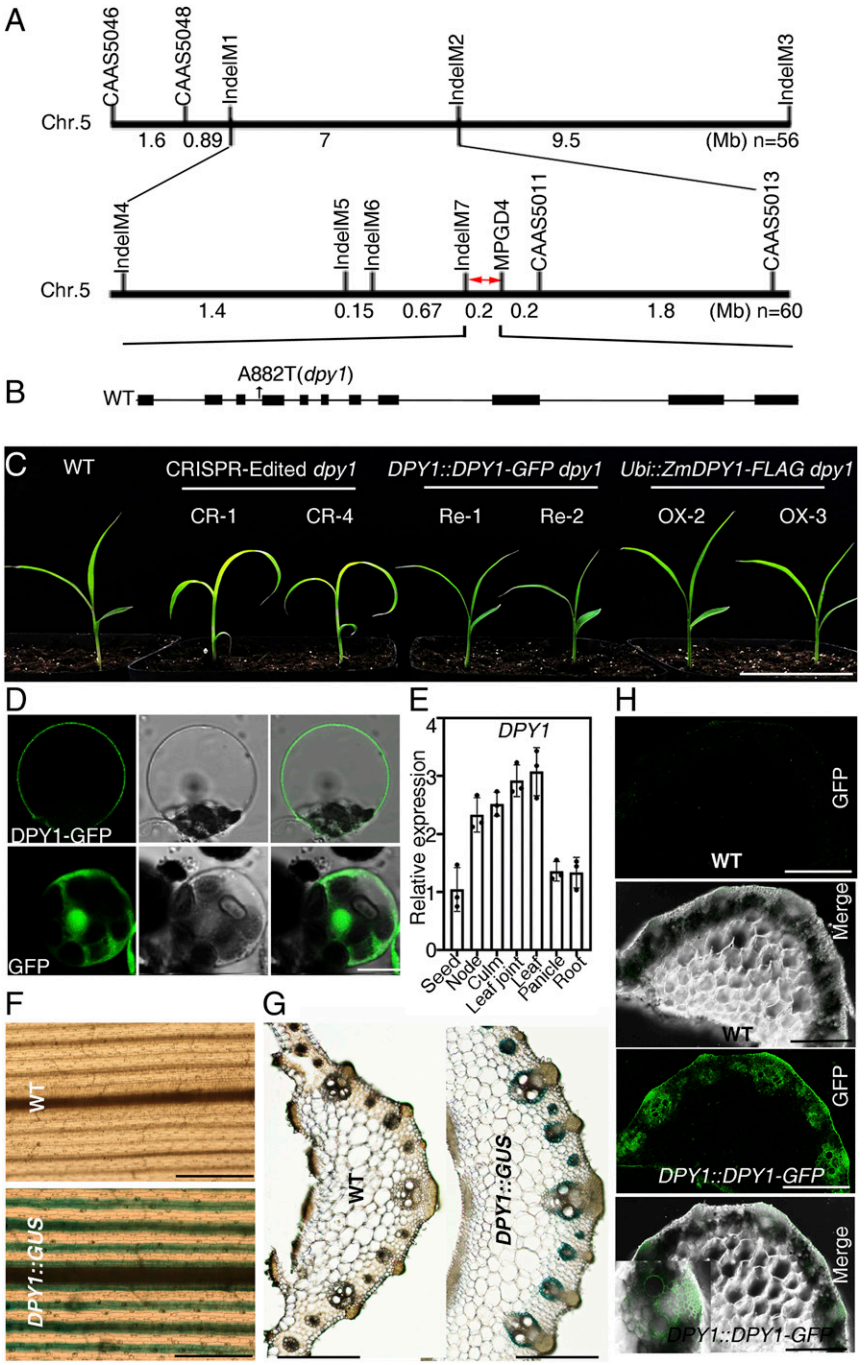

Fig. 2. *DPY1* encodes a plasma membrane-localized LRR kinase and is preferentially expressed in the vascular tissue. (*A*) Mapping of *dpy1*. Molecular markers and their corresponding physical distances to each other based on the Yugu1 reference genome are indicated. The *dpy1* locus was narrowed down to a 200-kb region between markers IndelM7 and MPGD4. (*B*) Genomic structure of *DPY1*. Black rectangles and lines indicate exons and introns, respectively. An A-to-T substitution in *dpy1* is indicated. (*C*) WT, CRISPR-edited, and rescued plants via the transformation of *dpy1* with a *DPY1* genomic fragment (*DPY1::DPY1-GFP*) or maize *DPY1* (*Ubi::ZmDPY1-FLAG*) at the seedling stage. (Scale bar, 10 cm.) (*D*) Plasma membrane localization of the DPY1-GFP fusion protein in a foxtail millet protoplast. A vector containing *GFP* alone was used as a control (*Lower*). (Scale bar, 10 μm.) (*E*) *DPY1* tissue-specific expression. The expression level in the seed was set as 1.0. Error bars indicate the SD ($n = 3$). (*F*) GUS staining of a leaf blade containing *DPY1::GUS*, showing GUS activity restricted to leaf veins. WT was used as a control. (Scale bar, 0.5 cm.) (*G*) Transverse section of a *DPY1::GUS* leaf blade, showing vascular tissue preferred promoter activity of *DPY1*. The WT was used as a control. (Scale bar, 25 μm.) (*H*) Confocal microscopy images of the cross-section from a leaf blade containing *DPY1::DPY1-GFP*, showing the GFP signals restricted to vascular tissues in the midrib. The WT was used as a control. (Scale bar, 50 μm.)

overlapped with that in *dpy1* (714 of 2,009 DEGs) (Fig. 4*E*), and nearly 80% of them had similar expression trends in both groups (Fig. 4 *F* and *G*). These findings support the repression of DPY1 in BR signaling in foxtail millet.

Additionally, we found down-regulation of most cyclin-like genes that have been shown to contribute to sclerenchyma cell proliferation in rice leaf joints (3) and of cell wall organization-related genes in *dpy1* and BL-treated WT plants (*SI Appendix*,

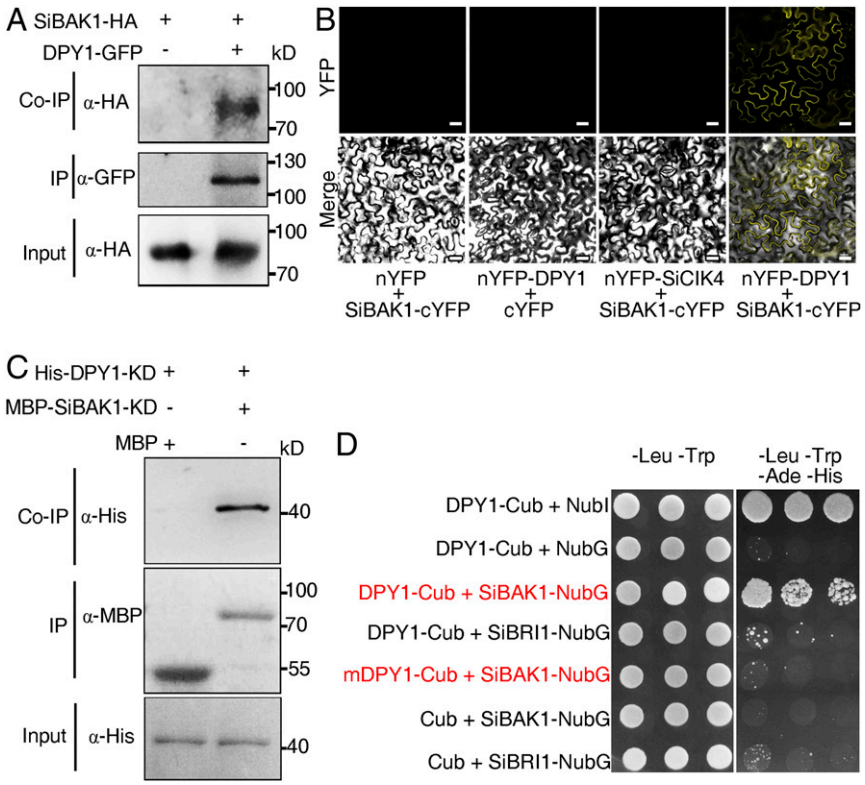

Fig. 3. DPY1 interacts with SiBAK1, but not SiBRI1, in a partial kinase-dependent manner. (*A*) The association between DPY1 and SiBAK1 was detected in a Co-IP assay. Protein extracts from protoplasts transiently expressing *35S::DPY1-GFP* and *35S::SiBAK1-HA* were immunoprecipitated with GFP-Trap beads (IP: α-GFP antibody) and immunoblotted with an α-HA antibody (Co-IP). (*B*) Interaction between DPY1 and SiBAK1 detected in a BiFC assay using tobacco epidermal cells. SiCIK4 (Seita.1G023400), a closely related protein with DPY1 in the LRRII-RKs subfamily (see *SI Appendix*, Fig. S6*A*), was used as a negative control. (Scale bar, 25 μm.) (*C*) An in vitro pull-down assay showing the interaction of DPY1 with SiBAK1 via kinase domains (KDs). The MBP or MBP-SiBAK1-KD proteins were incubated with the His-DPY1-KD protein and immunoprecipitated with MBP beads (IP) and immunoblotted with an α-His antibody (Co-IP). (*D*) DPY1 interacted with SiBAK1, but not with either SiBRI1 or mDPY1 (a dead version of DPY1, also see *SI Appendix*, Fig. S7*A*), in a DUAL-membrane yeast two-hybrid assay. Yeast growth is presented at three dilutions.

Fig. S11 *C* and *D*), while the *YABBY* genes that have been reported to regulate leaf droopiness in maize (1), were not differently expressed (fold change < 1.5; *SI Appendix*, Fig. S11*E*). Expression decline of those genes may account for the decreased sclerenchyma cell number and lignin deposition observed in *dpy1* (Fig. 1 *F* and *G* and *SI Appendix*, Table S1).

Finally, the supply of exogenous BL to *dpy1* seedlings resulted in severely curled leaf blades, while the treatment with BR synthesis inhibitor BRZ partially rescued its droopy leaf phenotype (Fig. 4 *H*–*J*). The differential responses from WT suggest enhanced BR signaling in *dpy1*. Collectively, these findings demonstrate that DPY1 prevents leaves from drooping by negatively regulating early BR signaling.

BL Treatment Enhances DPY1 Accumulation as Negative Feedback Regulation to Prevent SiBRI1 from Overactivation. The above results point to a regulatory loop mediated by DPY1 to orchestrate early BR signaling. To explore whether DPY1 is regulated by BR, the *DPY1* promoter activity change in response to BL treatment was probed in an 8-h time course experiment using transgenic *DPY1::DPY1-GFP dpy1* seedlings and found that *DPY1-GFP* transcript abundance was induced by BL, obviously starting at the 1-h time point and then remained steady afterward (*SI Appendix*, Fig. S12). Correspondingly, DPY1-GFP protein accumulation increased with BL treatment (Fig. 5*A* and *SI Appendix*, Fig. S13*A*). Moreover, we found higher DPY1 accumulation in the *Ubi::DPY1-3FLAG* plants subjected to the same time course BL treatment, suggesting that BR may also stabilize DPY1 (Fig. 5*B* and *SI Appendix*, Fig. S13*B*). Additionally, with SiBAK1-HA transiently expressed in protoplasts isolated from *Ubi::DPY1-3FLAG* transgenic plants, protein stabilization of DPY1-FLAG was enhanced relative to that of protoplasts expressing the vector control (Fig. 5*C* and *SI Appendix*, Fig. S13*C*). Given that *BAK1* overexpression enhances BR signaling (12, 13), and that DPY1 protein levels increase after BL treatment even under the *Ubiquitin* promoter (Fig. 5*B*), it is likely that transiently overexpressed SiBAK1 in protoplasts stabilizes DPY1 by enhancing BR signaling. These findings suggest that feedback loops may exist to regulate DPY1 expression and stability.

To further examine the negative modulation mechanism of DPY1, we conducted in vitro kinase activity assays to examine if DPY1 and SiBAK1 phosphorylate each other. The results showed that SiBAK1 could phosphorylate kinase-dead DPY1 (mDPY) but DPY1 could not phosphorylate kinase-dead SiBAK1 (mSiBAK1) (Fig. 5*D* and *SI Appendix*, Fig. S14*A*). Furthermore, the increased phosphorylation of DPY1 was detected in *Ubi::DPY1-3FLAG* transgenic plants treated with BL (Fig. 5*E* and *SI Appendix*, Fig. S14*B*). Since phosphorylation of DPY1 is critical for its interaction with SiBAK1 (Fig. 3*D* and *SI Appendix*, Fig. S7*B*), we proposed that BL-stimulated DPY1 phosphorylation would promote the DPY1–SiBAK1 interaction. A Co-IP assay with protoplasts coexpressing SiBAK1-HA and DPY1-GFP showed that BL treatment promoted the DPY1–SiBAK1 interaction, as indicated by the increase of coimmunoprecipitated SiBAK1 under BL treatment along with the same amount of immunoprecipitated DPY1 (Fig. 5*F* and *SI Appendix*, Fig. S15*A*). Similar results were

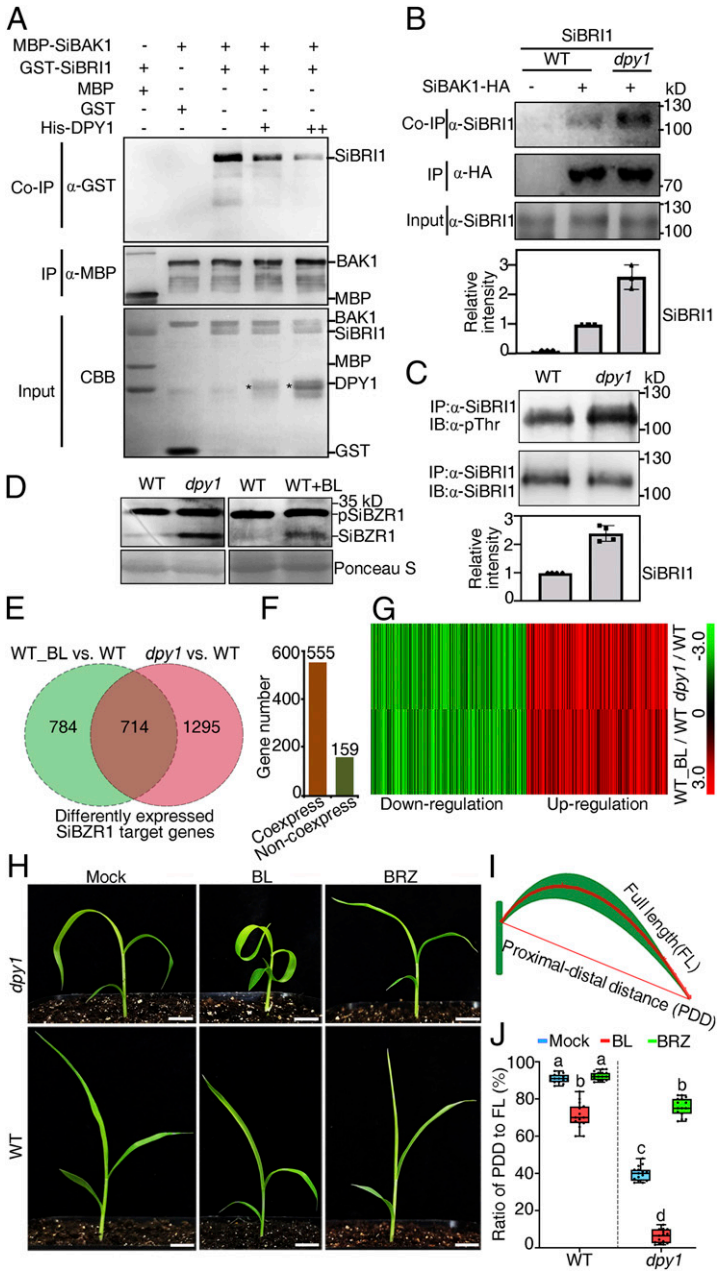

Fig. 4. DPY1 competes with SiBRI1 to bind SiBAK1 to repress BR signaling. (*A*) An in vitro pull-down assay indicated that DPY1 competes with SiBRI1 to bind to SiBAK1. The MBP-SiBAK1-KD (kinase domain) protein was incubated with the GST-SiBRI1-KD protein with various amounts of His-DPY1-KD and immunoprecipitated with MBP beads (IP) and immunoblotted with an α-GST antibody (Co-IP). MBP and GST were used as negative control proteins. Coomassie brilliant blue (CBB) staining of input proteins is presented at the *Bottom*. Asterisk indicates the band of His-DPY1-KD. (*B*) A Co-IP assay in the WT and *dpy1* protoplasts revealed the increased interaction between SiBAK1 and SiBRI1 in *dpy1*. Protein extracts from the WT or *dpy1* protoplasts transiently expressing *35S::SiBAK1-HA* or the vector control were immunoprecipitated with an α-HA antibody (IP) and immunoblotted with an α-SiBRI1 antibody (Co-IP), which had been validated (see *SI Appendix*, Fig. S8*A*). ImageJ was used to quantify signal intensity. Values represent the mean ± SD ($n = 3$). (*C*) Enhanced phosphorylation of endogenous SiBRI1 in *dpy1* plants. SiBRI1 was immunoprecipitated with an anti-SiBRI1 antibody (IP) and its phosphorylation status was determined by immunoblotting (IB) with an anti-pThr antibody. ImageJ was used to quantify signal intensity. Values represent mean ± SD ($n = 4$). (*D*) Immunoblots with an anti-OsBZR1 antibody that had been validated in foxtail millet (see *SI Appendix*, Fig. S8 *B* and *C*). Images indicate the increase in dephosphorylated SiBZR1 versus phosphorylated SiBZR1(SiBZR1-p) as a verification of enhanced BR signaling in *dpy1* due to more phosphorylated SiBRI1 observed in *C*. The WT plants were treated with 1 μM BL to simulate an enhancement of dephosphorylated SiBZR1 as a comparison. (*E*) Venn diagram of differentially expressed BZR1 target genes in *dpy1* and BL-treated WT plants relative to expression levels in untreated WT plants. A fold-change >2 ($P < 0.01$) was used as the cutoff. (*F*) Number of coexpressed (i.e., expression change in the same direction) and non-coexpressed genes among the 714 differentially expressed BZR1 target genes identified in both the WT_BL vs. WT and *dpy1* vs. WT comparisons. (*G*) Heatmap visualizing the expression patterns of the 555 differentially expressed BZR1 target genes that were coexpressed in the above two groups. (*H*) Responses to BR and BR synthesis inhibitor BRZ in WT and *dpy1* plants. Plants were treated with 5 μM BL or BRZ for 3 d. (Scale bar, 1 cm.) (*I*) Diagram illustrating the proximal-distal distance (PDD) and full length (FL) of a leaf blade. The PDD/FL ratio was used to measure curling degree of the leaf blade. (*J*) PDD/FL ratio of the second leaf from *Top* in WT and *dpy1* seedlings treated with mock, BL and BRZ, respectively. Error bars indicate the SD ($n = 15$). Different letters indicate significant differences at $P < 0.01$ by one-way ANOVA analysis.

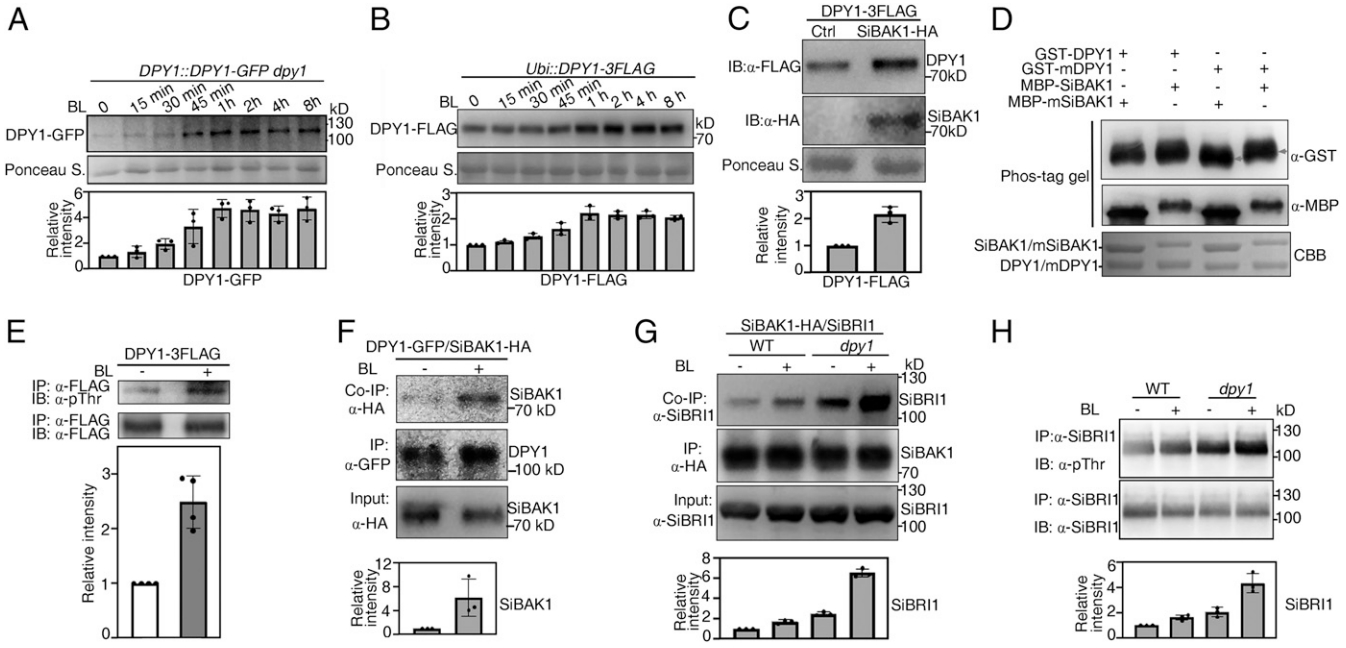

Fig. 5. BL treatment enhances DPY1 accumulation to prevent SiBRI1 overactivity. (*A* and *B*) BL-triggered accumulation of the DPY1-GFP and DPY1-FLAG proteins in *DPY1::DPY1-GFP dpy1* and *Ubi::DPY1-3FLAG* transgenic plants, respectively. Ponceau staining served as a loading control. Plants were treated with 5 μM BL at the indicated time period. ImageJ was used to quantify signal intensity. Values represent the mean ± SD ($n = 3$). (*C*) SiBAK1 stabilizes DPY1. The *35S::SiBAK1-HA* construct or the empty vector, as a control (Ctrl), was transiently expressed in *Ubi::DPY1-3FLAG* transgenic protoplasts for 12 h. Protein accumulation was analyzed by immunoblotting with α-HA or α-FLAG antibodies. ImageJ was used to quantify signal intensity. Values represent the mean ± SD ($n = 3$). (*D*) SiBAK1 phosphorylates DPY1. The MBP-SiBAK1-KD or its kinase-dead version MBP-mSiBAK1-KD protein was incubated with GST-DPY1-KD or GST-mDPY1-KD at 28 °C for 3 h in the presence of ATP. Phosphorylation of GST-mDPY1-KD was detected by the band shift in Phos-tag gel. The *Lower* presents the Coomassie brilliant blue (CBB) staining results for the corresponding recombinant proteins. The gray arrows indicate a shift of the band of mDPY1. (*E*) DPY1 phosphorylation is enhanced by BL. DPY1 from *Ubi::DPY1-3FLAG* transgenic plants treated with or without BL at 10 μM was immunoprecipitated (IP) with an α-FLAG antibody, and then the phosphorylation levels were detected with an anti-pThr antibody (IB). ImageJ was used to quantify signal intensity. Values represent the mean ± SD ($n = 4$). (*F*) BL enhances DPY1–SiBAK1 interaction. Protoplasts were cotransfected with *35S::DPY1-GFP* and *35S::SiBAK1-HA* for 12 h and incubated with 5 μM BL for 2 h. The Co-IP assay was completed as described in Fig. 3*A*. ImageJ was used to quantify signal intensity. Values represent mean ± SD ($n = 3$). (*G*) The BL-stimulated SiBRI1–SiBAK1 interaction is enhanced in *dpy1*. The *35S::SiBAK1-HA* construct was expressed in the WT and *dpy1* protoplasts for 12 h and incubated with or without 5 μM BL for 2 h. The Co-IP assay was completed as described in Fig. 4*B*. ImageJ was used to quantify signal intensity. Values represent the mean ± SD ($n = 3$). (*H*) BL-stimulated SiBRI1 phosphorylation is enhanced in *dpy1*. The *dpy1* and WT plants were treated with or without 5 μM BL. SiBRI1 was immunoprecipitated with an α-SiBRI1 antibody (IP) and its phosphorylation status was determined by immunoblotting with an α-pThr antibody (IB). ImageJ was used to quantify signal intensity. Values represent mean ± SD ($n = 3$).

also seen in a reverse Co-IP assay (*SI Appendix*, Fig. S15*B*). The dynamics of DPY1 interacting with SiBAK1 is different from that of other negative regulators of BR signaling, such as BAK1-INTERACTING RECEPTOR-LIKE KINASE 3 (BIR3), which is released from BAK1 upon BR perception (27). Nevertheless, the BL-enhanced DPY1–SiBAK1 interaction may raise the threshold of SiBRI1–SiBAK1 complex formation at the membrane.

Collectively, the above results revealed DPY1-mediated negative feedback regulation in early BR signaling. To further elucidate how such the regulation responses to BL treatment, we examined the SiBRI1–SiBAK1 interaction in the WT and *dpy1* in response to BL treatment by employing a Co-IP assay using WT or *dpy1* protoplasts expressing SiBAK1-HA treated with or without BL. The BL-stimulated SiBRI1–SiBAK1 interaction was more profound in *dpy1* than in the WT (Fig. 5*G* and *SI Appendix*, Fig. S16). Consequently, BL treatment led to more phosphorylation of SiBRI1 in *dpy1* (Fig. 5*H* and *SI Appendix*, Fig. S17). This is consistent with the observation that high-dose BL treatment results in more serious leaf droopiness in *dpy1*, relative to the WT (Fig. 4 *H*–*J*). Additionally, we detected much higher levels of endogenous BL content in foxtail millet leaves (*SI Appendix*, Table S3) than in other cereal crops (28, 29). This finding may highlight the importance of DPY1 in preventing BR signaling from overactivation caused by a high BL level in foxtail millet (*SI Appendix*, Fig. S18).

Discussion

In this study, we identified a member of the subfamily II of LRR-RKs, DPY1, which supports the upward architecture of leaves by regulating proper output of early BR signaling in *S. italica*. In a *DPY1* loss-of-function mutant, BR signaling is enhanced, and as a result, *dpy1* plants develop droopy leaves and are more susceptible to pathogen attack (*SI Appendix*, Fig. S2). Our findings highlight the trade-off between BR-mediated growth and plant innate immunity.

We have demonstrated that DPY1 competes with SiBRI1 for SiBAK1 interaction, and that BL treatment up-regulates DPY1 transcripts and DPY1 protein level (*SI Appendix*, Fig. S12 and Fig. 5 *A* and *B*). Therefore, there should be two layers of negative feedback regulation to keep normal BR activity from overactivation. On one hand, *DPY1* expression was promoted by BRs, particularly after 1 h of treatment (*SI Appendix*, Fig. S12), supporting the existence of a feedback loop from downstream signaling to DPY1 transcription. On the other hand, our results also suggest the existence of another feedback loop that stabilizes DPY1 and enhances DPY1–SiBAK1 affinity in the presence of excess BRs (Fig. 5 *B* and *F*). Further studies are needed to better understand the possible feedback mechanisms. Combining our data with the knowledge from the current literature, we hypothesize that DPY1 has a higher affinity than SiBRI1 to SiBAK1, which prevents SiBAK1 from interacting with SiBRI1 in the absence of BRs (*SI Appendix*, Fig. S18), as previously reported for BIR LRR receptor

pseudokinases (27, 30). In turn, SiBAK1 has higher affinity to BR-bound SiBRI1 than to DPY1, and thus, BR treatment is effective in creating an active BRI1–BAK1 complex. This is a high-affinity complex that is unlikely to dissociate and is probably internalized together. In a feedback loop, levels of DPY1 increase at the plasma membrane, which raises the threshold for SiBRI1–SiBAK1 complex formation, thus effectively damping BR signaling. In *dpy1*, the SiBRI1–SiBAK1 complex forms more easily (as more SiBAK1 is available) than in the WT and consequently, generates a stronger BR signaling response (*SI Appendix*, Fig. S18). This mechanism is reminiscent of recent reported findings, in which LRRII-RK NIK1, the homolog of DPY1 in *Arabidopsis*, interacts with BAK1 to reduce the formation of flg22-induced FLS2–BAK1 complexes, and thus, negatively regulates antibacterial immunity. Moreover, NIK1 is suggested to be a downstream target of the flg22-induced FLS2–BAK1 complex, which phosphorylates NIK1 to enhance NIK's affinity for FLS2 and BAK1 to inhibit constant immunity signaling activation (31). Thus, our findings indicate a common regulatory mechanism of NIK1/DPY1 over BAK1 that extends to multiple signaling pathways.

Notably, the loss of function in *DPY1* led to a severe disease phenotype (*SI Appendix*, Fig. S2). This finding points to a BR-involved trade-off between plant growth and immunity in response to environmental cues, as dark-grown *dpy1* seedlings display enhanced coleoptile elongation (Fig. 1*H*). DPY1 is closely related to NIK1, which plays a positive role in plant antiviral defense (32, 33), but a negative role in bacterial disease resistance by repressing FLS2–BAK1 complex formation upon flg22 perception (31). It is unknown if DPY1 also interacts with FLS2 but its positive role in mediating brown streak disease resistance, caused by the bacterial pathogen *Pseudomonas setariae*, suggests that DPY1 has evolved an innate immunity pathway different from NIK1. Alternatively, enhanced disease susceptibility in *dpy1* is most likely due to the increased BR signaling output leading to higher accumulation of activated SiBZR1 (Fig. 4*D*), which is shown to be crucial for the suppression of immunity by BR (34). BR-PTI (pathogen-associated molecular pattern-triggered immunity) cross-talk at BZR1, independent of BAK1, has been well documented, at which plants balance the trade-off of resource allocation for growth or defense against diseases (34, 35). Considering that the *dpy1* plants are supposed to have more SiBAK1 proteins available to bind other PAMP (pathogen-associated molecular pattern) receptors, such as FLS2 homologs, but are more susceptible to bacterial pathogen attack, we propose that DPY1 mediates disease resistance independent of the SiBAK1-dependent immune pathway, at least for brown streak disease. It would be interesting to investigate if DPY1-overexpressing plants also gain disease resistance, in addition to the observed improvement of leaf architecture and potential yield increase.

We have demonstrated that *DPY1*-overexpressing plants exhibit an improved plant architecture with upright leaf blades, increased stem width, and yield per plant (*SI Appendix*, Fig. S5). Thus, *DPY1* may be relevant for cereal crop breeding. Moreover, a maize *DPY1* homolog fully rescues leaf droopiness of the *dpy1* mutant (Fig. 2*C*), suggesting that the regulatory function of *DPY1* regarding leaf droopiness is conserved among species. Therefore, *DPY1* represents a candidate gene for the breeding of crops with an enhanced plant architecture and yield. Our study data provide cellular and molecular insights related to the plant architecture in cereals.

Materials and Methods

A detailed description of plant materials, growth condition, map-based cloning of *DPY1*, bioinformatics analysis of *DPY1*, paraffin section, vector construction, plant transformation, RNA-seq analysis, protein–protein interaction assays, and associated references is available in *SI Appendix, Materials and Methods*.

Data Availability. RNA sequencing raw data were deposited into the European Nucleotide Archive under accession number PRJEB31229. The primers used in this study are listed in Dataset S1. Other study data are included in the article and supporting information.

ACKNOWLEDGMENTS. We thank Chengcai Chu (Institute of Genetics and Developmental Biology, Chinese Academy of Sciences), Xuelu Wang (Huazhong Agricultural University), and Rae Eden Yumul for critical discussion of this work. We thank Jun Liu (Institute of Crop Sciences, Chinese Academy of Agricultural Sciences) for revising the working model. This work was supported by the National Key Research and Development Program of China (2018YFD1000706/2018YFD1000700 to M.Z. and 2016YFD0100400 to Xigang Liu); the National Natural Science Foundation of China (31871634 to M.Z., 31671354 to Xigang Liu, 31771807 to X.D., and 31770398 to J.C.); the China Agricultural Research System (CARS-06-A4); Science and Technology Innovation Project of Chinese Academy of Agricultural Science (Team of Minor Cereal and Legumes; No. CAAS-ZDXT2019003); Fundamental Research Funds of Chinese Academy of Agricultural Science (S2018PY03 to S.T.); the Natural Science Foundation of Hebei province (C2020503004 to M.Z.); the Key Research Program of the Chinese Academy of Science (KFZD-SW-112); and Science and Technology Service Network Initiative of Chinese Academy of Sciences (KFJ-STS-ZDTP-024).

1. J. Strable *et al.*, Maize *YABBY* genes *drooping leaf1* and *drooping leaf2* regulate plant architecture. *Plant Cell* **29**, 1622–1641 (2017).
2. J. Tian *et al.*, Teosinte ligule allele narrows plant architecture and enhances high-density maize yields. *Science* **365**, 658–664 (2019).
3. S. Sun *et al.*, Brassinosteroid signaling regulates leaf erectness in Oryza sativa via the control of a specific U-type cyclin and cell proliferation. *Dev. Cell* **34**, 220–228 (2015).
4. H. Tong, C. Chu, Functional specificities of brassinosteroid and potential utilization for crop improvement. *Trends Plant Sci.* **23**, 1016–1028 (2018).
5. T. Yamaguchi *et al.*, The *YABBY* gene *DROOPING LEAF* regulates carpel specification and midrib development in *Oryza sativa*. *Plant Cell* **16**, 500–509 (2004).
6. M. I. Stahle, J. Kuehlich, L. Staron, A. G. von Arnim, J. F. Golz, YABBYs and the transcriptional corepressors LEUNIG and LEUNIG_HOMOLOG maintain leaf polarity and meristem activity in Arabidopsis. *Plant Cell* **21**, 3105–3118 (2009).
7. T. M. Nolan, N. Vukašinović, D. Liu, E. Russinova, Y. Yin, Brassinosteroids: Multidimensional regulators of plant growth, development, and stress responses. *Plant Cell* **32**, 295–318 (2020).
8. Z. Y. Wang, M. Y. Bai, E. Oh, J. Y. Zhu, Brassinosteroid signaling network and regulation of photomorphogenesis. *Annu. Rev. Genet.* **46**, 701–724 (2012).
9. Z. Y. Wang, H. Seto, S. Fujioka, S. Yoshida, J. Chory, BRI1 is a critical component of a plasma-membrane receptor for plant steroids. *Nature* **410**, 380–383 (2001).
10. J. Santiago, C. Henzler, M. Hothorn, Molecular mechanism for plant steroid receptor activation by somatic embryogenesis co-receptor kinases. *Science* **341**, 889–892 (2013).
11. Y. Sun *et al.*, Structure reveals that BAK1 as a co-receptor recognizes the BRI1-bound brassinolide. *Cell Res.* **23**, 1326–1329 (2013).
12. J. Li *et al.*, BAK1, an Arabidopsis LRR receptor-like protein kinase, interacts with BRI1 and modulates brassinosteroid signaling. *Cell* **110**, 213–222 (2002).
13. K. H. Nam, J. Li, BRI1/BAK1, a receptor kinase pair mediating brassinosteroid signaling. *Cell* **110**, 203–212 (2002).
14. D. Bojar *et al.*, Crystal structures of the phosphorylated BRI1 kinase domain and implications for brassinosteroid signal initiation. *Plant J.* **78**, 31–43 (2014).
15. U. Hohmann, K. Lau, M. Hothorn, The structural basis of ligand perception and signal activation by receptor kinases. *Annu. Rev. Plant Biol.* **68**, 109–137 (2017).
16. X. Wang *et al.*, Sequential transphosphorylation of the BRI1/BAK1 receptor kinase complex impacts early events in brassinosteroid signaling. *Dev. Cell* **15**, 220–235 (2008).
17. X. Wang, J. Chory, Brassinosteroids regulate dissociation of BKI1, a negative regulator of BRI1 signaling, from the plasma membrane. *Science* **313**, 1118–1122 (2006).
18. W. Tang *et al.*, BSKs mediate signal transduction from the receptor kinase BRI1 in *Arabidopsis*. *Science* **321**, 557–560 (2008).
19. T. W. Kim *et al.*, Brassinosteroid signal transduction from cell-surface receptor kinases to nuclear transcription factors. *Nat. Cell Biol.* **11**, 1254–1260 (2009).
20. Y. Yin *et al.*, BES1 accumulates in the nucleus in response to brassinosteroids to regulate gene expression and promote stem elongation. *Cell* **109**, 181–191 (2002).
21. H. Ryu *et al.*, Nucleocytoplasmic shuttling of BZR1 mediated by phosphorylation is essential in Arabidopsis brassinosteroid signaling. *Plant Cell* **19**, 2749–2762 (2007).
22. G. Wu *et al.*, Methylation of a phosphatase specifies dephosphorylation and degradation of activated brassinosteroid receptors. *Sci. Signal.* **4**, ra29 (2011).
23. R. Wang *et al.*, The brassinosteroid-activated BRI1 receptor kinase is switched off by dephosphorylation mediated by cytoplasm-localized PP2A B′ subunits. *Mol. Plant* **9**, 148–157 (2016).
24. P. Li, T. P. Brutnell, Setaria viridis and Setaria italica, model genetic systems for the Panicoid grasses. *J. Exp. Bot.* **62**, 3031–3037 (2011).

25. X. Diao, J. Schnable, J. L. Bennetzen, J. Li, Initiation of Setaria as a model plant. *Front. Agric. Sci. Eng.* **1**, 16–20 (2014).
26. T. Halter *et al*., The leucine-rich repeat receptor kinase BIR2 is a negative regulator of BAK1 in plant immunity. *Curr. Biol.* **24**, 134–143 (2014).
27. J. Imkampe *et al*., The Arabidopsis leucine-rich repeat receptor kinase BIR3 negatively regulates BAK1 receptor complex formation and stabilizes BAK1. *Plant Cell* **29**, 2285–2303 (2017).
28. P. Xin, J. Yan, J. Fan, J. Chu, C. Yan, An improved simplified high-sensitivity quantification method for determining brassinosteroids in different tissues of rice and Arabidopsis. *Plant Physiol.* **162**, 2056–2066 (2013).
29. A. Bajguz, W. Orczyk, A. Gołębiewska, M. Chmur, A. Piotrowska-Niczyporuk, Occurrence of brassinosteroids and influence of 24-epibrassinolide with brassinazole on their content in the leaves and roots of Hordeum vulgare L. cv. Golden Promise. *Planta* **249**, 123–137 (2019).
30. U. Hohmann, J. Nicolet, A. Moretti, L. A. Hothorn, M. Hothorn, The SERK3 elongated allele defines a role for BIR ectodomains in brassinosteroid signalling. *Nat. Plants* **4**, 345–351 (2018).
31. B. Li *et al*., The receptor-like kinase NIK1 targets FLS2/BAK1 immune complex and inversely modulates antiviral and antibacterial immunity. *Nat. Commun.* **10**, 4996 (2019).
32. C. M. Carvalho *et al*., Regulated nuclear trafficking of rpL10A mediated by NIK1 represents a defense strategy of plant cells against virus. *PLoS Pathog.* **4**, e1000247 (2008).
33. C. Zorzatto *et al*., NIK1-mediated translation suppression functions as a plant antiviral immunity mechanism. *Nature* **520**, 679–682 (2015).
34. R. Lozano-Durán *et al*., The transcriptional regulator BZR1 mediates trade-off between plant innate immunity and growth. *eLife* **2**, e00983 (2013).
35. C. Albrecht *et al*., Brassinosteroids inhibit pathogen-associated molecular pattern-triggered immune signaling independent of the receptor kinase BAK1. *Proc. Natl. Acad. Sci. U.S.A.* **109**, 303–308 (2012).